Phase Behavior of Poly(vinyl methyl ether) in Deuterium Oxide

Kurt Van Durme,[†] Els Loozen,[‡] Erik Nies,[*,‡,§] and Bruno Van Mele[*,†]

Department of Physical Chemistry and Polymer Science, Vrije Universiteit Brussel, Brussels, Belgium; Polymer Research Division, Department of Chemistry, Katholieke Universiteit Leuven, Leuven, Belgium; and Laboratory of Polymer Technology, Eindhoven University of Technology, Eindhoven, The Netherlands

Received August 5, 2005; Revised Manuscript Received September 27, 2005

ABSTRACT: The Wertheim lattice thermodynamic perturbation theory is used to calculate the liquid−liquid and solid−liquid coexistence data of a model polymer solution. The theory predicts bimodal LCST phase behavior as well as an unusual step with composition in the solid−liquid equilibrium of the solvent. These theoretical predictions are discussed in relation to the experimental results obtained for the poly(vinyl methyl ether) (PVME)/D_2O system. The apparent heat capacity signal from modulated temperature DSC (MTDSC) is used to measure the onset of LCST phase separation along with the melting temperature of D_2O in the presence of PVME. The experimentally observed trace of the melting endotherm allows calculating the complete melting line of the solvent, in agreement with theory. Moreover, an alternative approach, employing Fourier transform infrared spectroscopy, is established from which the equilibrium melting line of D_2O could be determined, again confirming theoretical predictions. The peculiar concentration dependence of the melting curve of ice provides a new explanation for (i) the double melting endotherm observed in (MT)DSC and (ii) the inhibited crystallization in highly concentrated aqueous PVME mixtures. Finally, the existence of a low-temperature UCST miscibility gap is suggested via an insightful examination of the glass transition region.

Introduction

Aqueous polymer systems have attracted considerable interest as they may exhibit large, reversible conformational changes in response to small environmental stimuli (e.g., temperature, pH, electrical field, pressure, light, etc.), causing a change in physical or chemical properties.[1] Hence, such polymeric materials can be applied in numerous fields.[2−6] Thermoresponsive water-soluble polymers are frequently characterized by a lower critical solution temperature (LCST) miscibility behavior, which implies that the linear polymer dissolves in water at low temperature and phase separates from the aqueous solution upon heating. Accordingly, depending on the specific LCST phase behavior of the polymer, the cross-linked analogues may show an order-of-magnitude shrinking in hydrogel size upon raising the temperature.[7−12]

Poly(vinyl methyl ether) (PVME) shows a type III LCST partial miscibility behavior in water at physiological temperatures, according to a classification of polymer/solvent phase diagrams.[7] This atypical LCST phase behavior consists of two lower two-phase areas separated from one upper two-phase area by a three-liquid-phases coexistence line at invariant temperature.[13] Consequently, the PVME/water system displays two stable liquid−liquid critical points: one which obeys the classical Flory−Huggins (FH) theory, i.e., it decreases with increasing polymer molar mass, and a second one (at high PVME concentration), which is nearly molar mass independent.[8]

The LCST demixing process consists of breaking hydrogen bonds together with large compositional changes, accompanied by a significant endothermic heat effect that can be studied by differential scanning calorimetry (DSC). Using conventional DSC, a complex thermal behavior with two overlapping endothermic peaks is observed, reflecting the shape of the bimodal demixing curve.[14−16] At first, the sample is heated through a two-phase region, which is seen as a broad shoulder prior to a large peak with a maximum at ca. 37 °C, caused by large changes in composition upon passing the temperature at the three-phase equilibrium. The second peak is therefore often used to estimate the temperature at which three liquid phases coexist. Next to the LCST miscibility behavior, aqueous PVME solutions have also been investigated at subzero temperatures, especially focusing on the crystallization/melting properties of water.[15,17,18] These studies revealed that the melting endotherm of ice, using DSC, consists of two overlapping peaks (see, for instance, Figures 3 and 4 in ref 17). In the case of aqueous poly(ethylene oxide) (PEO) solutions, for instance, such a double melting endotherm is caused by the presence of a eutectic composition.[19,20] This explanation does not hold for the PVME/water system, since PVME is atactic and thus unable to crystallize. The most frequently adapted interpretation of the double melting peak in PVME/water mixtures refers to the existence of both water belonging to a stable polymer/solvent complex and free water, which melt at different temperatures.[17,18] Moreover, in highly concentrated mixtures (with mass fraction of PVME, $w_{PVME} > 0.6$) the crystallization of water does not occur when cooling at typical cooling rates used in e.g. DSC experiments. Similar observations hold for aqueous solutions of both poly(*N*-isopropylacrylamide) (PNIPAM)[10,21] and poly(*N*-vinylcaprolactam) (PVCL),[11] for which the missing crystallization of water at high polymer concentration results from the interference of the crystallization process with the vitrification of the homogeneous solution. Since PVME has a much lower glass transition temperature (ca. −25 °C), the arrested crystallization of water in the PVME/water system was

[†] Vrije Universiteit Brussel.
[‡] Katholieke Universiteit Leuven.
[§] Eindhoven University of Technology.
* Corresponding authors. E.N.: Fax +31-(0)40-2474954, Ph +31-(0)40-2474954, e-mail erik.nies@chem.kuleuven.be. B.V.M.: Fax +32-(0)2-6293278, Ph +32-(0)2-6293288, e-mail bvmele@vub.ac.be.

10.1021/ma051745y CCC: $30.25
Published on Web 10/27/2005

not ascribed to vitrification, but was again interpreted to give evidence to the existence of a stable molecular complex in which two water molecules are hydrogen bonded to the polymer repeating unit.[15]

However, further investigation of highly concentrated PVME/water mixtures demonstrated that for $w_{PVME} = 0.7$ the crystallization of water could be realized once ice nuclei are added.[18] This experiment casts doubt on the existence of stable molecular complexes and indicates that the arrested crystallization of water in highly concentrated mixtures is related to ice nucleation problems. However, for a conventional course of the melting line, nucleation problems seem quite unexpected as a sufficient supercooling in such mixture should be achievable, triggering nucleation and subsequent crystallization before the vicinity of the glass transition region slows down these processes.

Recent theoretical calculations for a model polymer solution containing saturation interactions (i.e., solvent−solvent and solvent−polymer) using the thermodynamic perturbation theory of Wertheim,[22−24] adapted to the lattice model,[25] provided more understanding on a molecular level of such peculiar liquid−liquid and solid−liquid phase behavior. That is to say, using the Wertheim lattice thermodynamic perturbation theory (Wertheim-LTPT) bimodal LCST miscibility is predicted in agreement with experimental observation.[25,26] Such theoretical prediction of bimodal phase behavior has previously not been realized, even though it could be phenomenologically described with an extended composition- and temperature-dependent Flory−Huggins interaction function.[26] In addition to the bimodal LCST phase behavior, and closely connected to it, two adjacent narrow upper critical solution temperature (UCST) miscibility gaps at low temperature were predicted.[26,27] Recently, the low-temperature UCST at high polymer concentration has been observed using small-angle neutron scattering (SANS).[26] Moreover, the calculated melting line of the solvent displays an unusual change with composition, which becomes more pronounced when the equilibrium melting temperature of the pure solvent is located at lower temperatures. This peculiar concentration dependence of the melting line of water was also experimentally confirmed using modulated temperature DSC (MTDSC) and FTIR.[27] Consequently, these theoretical predictions and experimental findings provide a new explanation for the inhibited crystallization at high polymer concentration, compared to the previously suggested molecular complex.[15,17,18]

In the present work, we will evaluate the phase behavior of PVME in deuterium oxide compared to the previously discussed undeuterated aqueous system. Mixtures of PVME and D_2O were already investigated using nuclear magnetic resonance (NMR) spectroscopy[28] and SANS.[26,29−32] Here, the phase behavior of PVME/D_2O mixtures is further investigated by means of MTDSC and FTIR with the emphasis on (i) providing more detailed, accurate experimental data and (ii) to put these data in relation to the aforementioned predictions of the Wertheim-LTPT. More specifically, the crystallization and melting behavior of D_2O will be thoroughly examined using MTDSC, considering the location of the glass transition temperature (T_g)−composition curve. Finally, the equilibrium melting line of D_2O is also determined with FTIR. Throughout the text, experimental data are discussed (qualitatively) in terms of the Wertheim-LTPT.

Experimental Section

Materials. Poly(vinyl methyl ether) (PVME) dissolved in water (mass fraction PVME, $w_{PVME} = 0.5$) was purchased from Aldrich Chemical Co. Inc. (mass average molar mass, $M_w = 20$ kg mol^{-1}, determined from SANS;[26] polydispersity, $M_w/M_n \sim 2.5$, derived from gel permeation chromatography (GPC)). To obtain the pure polymer, the mixture was diluted with deionized water to $w_{PVME} = 0.1$. This solution was heated to ca. 50 °C to induce liquid−liquid demixing. The concentrated phase was isolated and dried at 40 °C under vacuum for several days, until the water mass fraction was less than 0.005 as determined by thermogravimetric analysis (TA Instruments TGA 2950). The glass transition temperature of dried PVME is −25 °C.

D_2O (99.9 at. % deuterium) was obtained from Aldrich Chemical Co. Inc. and was used as received.

Sample Preparation. *MTDSC Experiments.* A range of compositions were prepared by adding the appropriate amount of D_2O to dried PVME directly in Mettler aluminum pans that were subsequently hermetically sealed. The inserted sample mass typically varied between 0.5 and 5 mg. Mixture compositions are expressed in mass fraction PVME in the PVME/D_2O mixture, w_{PVME}. These samples were stored at 4 °C for at least 3 weeks to obtain homogeneous mixtures. A few of the closed crucibles were perforated, and the water evaporation was measured at 100 °C to check the preparation procedure using TGA (error on polymer mass fraction is <0.001).

FTIR Experiments. A range of homogeneous mixtures of PVME and deuterium oxide were prepared by adding appropriate amounts of D_2O to dried PVME. These mixtures were regularly mechanically mixed (using closed recipients) and allowed to homogenize at room temperature for periods up to 2 months (for the highest polymer concentrations).

Experimental Methods. *Modulated Temperature Differential Scanning Calorimetry (MTDSC).* A first series of MTDSC measurements were performed on a TA Instruments 2920 DSC with the MDSC option and a refrigerated cooling system. Helium was used as a purge gas (25 mL min^{-1}). Indium and cyclohexane were used for temperature calibration. The former was also used for enthalpy calibration. Standard modulation conditions are an amplitude A_T of 0.50 °C with a period p of 60 s. Heat capacity calibration was performed in standard modulation conditions with water, using the heat capacity difference between two temperatures: one above and one below the melting temperature. In this way, the most accurate measurements of heat capacity changes and "excess" contributions, c_p^{excess}, were obtained. Data are expressed as specific heat capacities (or changes) in J g^{-1} K^{-1}. Nonisothermal experiments were performed at an underlying heating/cooling rate of 1 °C min^{-1}.

A second series of MTDSC experiments were performed on a TA Instruments Q1000 (T-zero DSC-technology) with a liquid nitrogen cooling system. The calibration conditions were as stated above. Nitrogen was used as a purge gas (25 mL min^{-1}).

Fourier Transform Infrared Spectroscopy (FTIR). A Perkin-Elmer FTIR 2000 spectrometer was used. The sample solutions were put between two calcium fluoride (CaF_2) windows, pressed together attaining IR absorbance readings below 1 (to ensure nonsaturated IR signals) and placed in a temperature-controlled cell (SPECAC). Temperature control was achieved by connecting the cell to a Julabo thermostat bath. A thermocouple attached to the temperature cell was used to attain accurate temperature readings. The background spectrum was obtained using a blank CaF_2 window. Ten interferograms, taken with a spectral resolution of 2 cm^{-1}, were superimposed to obtain a good signal-to-noise ratio. The standard deviations in temperature and reading of the FTIR wavenumbers are estimated to be 0.1 °C and 1 cm^{-1}, respectively.

Theoretical Section

The Wertheim Lattice Thermodynamic Perturbation Theory. From a theoretical point of view, it is of interest to investigate the complicated phase behavior

of systems involving hydrogen-bonding interactions using a theoretical approach that incorporates directly and explicitly the formation of specific interactions. In this respect, we apply the seminal work of Wertheim regarding saturation interactions, whereby the Wertheim theory is mapped onto the lattice model, which forms the basis of the Flory–Huggins theory as well.[22–25] Here we summarize the essential equations needed to describe the phase behavior. Details about the Wertheim-LTPT can be found elsewhere.[25]

The lattice positions, N_L in total, have coordination number z and are occupied either by a solvent molecule (component 0) or by a segment of a polymer molecule (component 1). Each molecule of component 0 carries a specific site A, and each segment of component 1 carries a specific site B. Nearest-neighbor molecules and segments interact by dispersive interactions with an interaction energy, $-\epsilon_{ij}$ $(i, j = 0, 1)$, depending on the pair of units (solvent molecules or polymer segments) involved. Furthermore, the specific sites A on molecules of type 1 interact with interaction strength ϵ_{00}^{AA} if they are properly oriented relative to each other and specific sites A and B interact with interaction strength $-\epsilon_{00}^{AA} = -\epsilon_{20}^{BA}$. No specific interaction exists between sites B, i.e., $\epsilon_{11}^{BB} = 0$.

In the lattice thermodynamic perturbation theory of Wertheim the excess Gibbs energy per lattice site can be written as a sum, according to

$$\Delta G/N_L kT = \Delta G_R/N_L kT + \Delta G_{NN}/N_L kT + \Delta G_{AB}/N_L kT \tag{1}$$

with k the Boltzmann constant and T the absolute temperature. The excess Gibbs energy of the reference system ΔG_R is the excess free enthalpy of the same system excluding both nearest-neighbor and specific interactions. Accordingly, using the Wertheim-LTPT, the Flory–Huggins combinatorial entropy is recovered:

$$\frac{\Delta G_R}{N_L kT} = \phi_0 \ln \phi_0 = \frac{\phi_1}{s_1} \ln \phi_1 \tag{2}$$

with s_1 the number of segments in a polymer chain and ϕ_i the segment fraction of component i.

The free energy of nearest-neighbor interactions is described using following mean-field approximation:

$$\frac{\Delta G_R}{N_L kT} = \frac{z\Delta w}{2kT}\phi_0\phi_1 = \chi\phi_0\phi_1 \tag{3}$$

with χ the Flory–Huggins interaction parameter and $\Delta w = 2(-\epsilon_{01}) - ((-\epsilon_{00}) + (-\epsilon_{11}))$, the exchange energy, defined for the nearest-neighbor dispersive interactions, which is the only relevant energy scale in the FH theory. This FH exchange energy allows defining a reduced temperature $T^* = 2kT/z\Delta w$, which will be used during calculation and for the representation of the predictions made. The sum of eqs 2 and 3 constitutes the standard Flory–Huggins mixture or solution theory in its most simple mean-field approximation. Although the simple FH theory does not provide a quantitative prediction of the actual phase behavior of the model system, it does capture its essence.

The excess free enthalpy due to associations between A sites and A and B sites is given by

$$\frac{\Delta G_{AB}}{N_L kT} = \phi_0\left[\ln X_A^0 - \frac{X_A^0}{2} + \frac{1}{2}\right] + \phi_1\left[\ln X_B^1 - \frac{X_B^1}{2} + \frac{1}{2}\right] \tag{4}$$

with X_A^0 (X_B^1) the fraction of nonbonded site A (B). These fractions are determined from the set of equations

$$\begin{aligned} \bar{X}_A(1 + \bar{X}_A\Delta_{AA} + \bar{X}_B\Delta_{AB}) - \phi_0 = 0 \\ \bar{X}_B(1 + \bar{X}_B\Delta_{AB} + \bar{X}_B\Delta_{BB}) - \phi_0 = 0 \end{aligned} \tag{5}$$

with $\bar{X}_A = \phi_0 X_A^0$ and $\bar{X}_B = \phi_1 X_B^1$.

The parameters $\Delta_{\alpha\beta}$ (α, β = A or B) in eq 5 are given by

$$\Delta_{\alpha\beta} = K(\exp(\epsilon_{ij}^{\alpha\beta}/kT) - 1) \tag{6}$$

with K the ratio of the nearest-neighbor positions with the proper orientation to all possible orientations.

Liquid–Liquid Equilibrium Calculations. Thermodynamic properties are easily derived from the excess Gibbs energy given by eq 1. In particular, spinodal and critical conditions can be calculated from the second and third compositional derivative of the free energy:

$$J_{sp} = \frac{\partial^2 \Delta G/N_L kT}{\partial {\phi_1}^2}\Big|_{T,p} = 0 \quad \text{and} \quad J_{cr} = \frac{\partial^3 \Delta G/N_L kT}{\partial {\phi_1}^3}\Big|_{T,p} = 0 \tag{7}$$

The critical temperature and composition are given by the simultaneous set of both equations, while the spinodal condition is solely governed by $J_{sp} = 0$. The liquid–liquid coexistence curves are calculated using the standard equilibrium conditions:

$$\Delta\mu_0' = \Delta\mu_0'' \quad \text{and} \quad \Delta\mu_1' = \Delta\mu_1'' \tag{8}$$

with $\Delta\mu_0'^{(\prime)}$ and $\Delta\mu_1'^{(\prime)}$ the excess chemical potential of the solvent (0) and polymer (1) in the coexisting liquid mixture phases, denoted by single and double primes. The excess chemical potential of component i, $\Delta\mu_i$, in the polymer solution can be calculated from the excess Gibbs energy, according to the standard thermodynamic definition $\Delta\mu_i = \left.\frac{\partial \Delta G}{\partial N_i}\right|_{T,p,N_j \neq N_i}$.

Solid–Liquid Equilibrium Calculations. The melting temperature of the crystalline solvent in equilibrium with a liquid polymer/solvent mixture can be calculated from the equilibrium condition:

$$\Delta\mu_0 = \Delta\mu_{0,solid}^0 \tag{9}$$

with $\Delta\mu_0(\Delta\mu_{0,solid}^0)$ the excess chemical potential of the solvent in the liquid mixture (pure solid crystalline) phase. To obtain the excess chemical potential $\mu_{0,solid}^0$ of

the pure crystalline solvent at the temperature $T_{m,0}$, we adapt the standard thermodynamic model:

$$\frac{\Delta\mu^0_{0,\text{solid}}}{kT_{m,0}} = \frac{\Delta H^0_{m,0}}{k}\left(\frac{1}{T^0_{m,0}} - \frac{1}{T_{m,0}}\right) = \frac{\Delta H^0_{m,0}}{z\Delta w/2}\left(\frac{z\Delta w/2}{kT^0_{m,0}} - \frac{z\Delta w/2}{kT_{m,0}}\right) = \Delta H^{0\,*}_{m,0}\left(\frac{1}{T^{0\,*}_{m,0}} - \frac{1}{T^{0\,*}_{m,0}}\right) \quad (10)$$

with $\Delta H^0_{m,0}$ and $T^0_{m,0}$ the enthalpy of melting and the equilibrium melting temperature of component 0, respectively. The third equality in eq 10 defines the reduced enthalpy of melting together with the reduced melting temperatures.

Equations 1−10 will be used to calculate the liquid−liquid miscibility behavior and the solid−liquid coexistence line.

Results and Discussion

The Wertheim Lattice Thermodynamic Perturbation Theory: Theoretical Phase Behavior for a Model Polymer Solution. In Figure 1 the predicted bimodal LCST binodal, spinodal, and critical conditions are shown. The parameters used for these predictions are collected in Table 1. It is the first time bimodal

Table 1. Phase Behavior of Poly(vinyl methyl ether) in Deuterium Oxide

parameter	value	parameter	value
s_1	100	K^{AA}_{00}	6
z	6	K^{BB}_{022}	6
ϵ_{01}/k	−0.1	$K^{AB}_{02} = K^{BA}_{20}$	495
$\epsilon_{00}/k = \epsilon_{11}/k$	0	$\Delta H^0_{m,0}{}^*$	1.500
ϵ^{AA}_{00}/k	1.5	$T^0_{m,0}{}^*$	0.200 0.225 0.250
$\epsilon^{AB}_{00}/k = \epsilon^{BA}_{11}/k$	2.8		

LCST phase behavior is predicted by theory. So far bimodality in aqueous solutions of PVME was only described phenomenologically with an extended composition and temperature-dependent Flory−Huggins interaction function.[26] Other theoretical approaches are available, but most of them address the problem of bimodality in a semiempirical way; i.e., additional terms are added to ascertain a sufficiently pronounced concentration dependence of the interaction function used, which makes the description of multiple critical points feasible.[33−36] More recently, a different approach was applied, handling the issue of multiple critical points in bimodal phase behavior. This approach focuses on the effects of inhomogeneous segment distribution in dilute polymer solutions and conformational changes in response to the solution environment. In this way, the criteria for the occurrence of multiple critical points could be defined, giving a molecular basis for the required concentration dependence of the interaction function.[37] In the present paper, however, a different route is elaborated, incorporating directly the occurrence of hydrogen bonding (saturation interactions) in the theory based on the seminal work of Wertheim.

The bimodal miscibility gap, derived from the Wertheim-LTPT, strongly depends on the interaction strength of the saturation interactions between solvent molecules compared to the strength of the saturation interactions between polymer segments and solvent molecules.[25] Bimodality is only observed when the solvent−polymer strength is (somewhat) larger than the solvent−solvent strength, i.e., when the values of the parameters $\epsilon^{\alpha\beta}_{ij}$ are chosen properly within certain bounds. The values

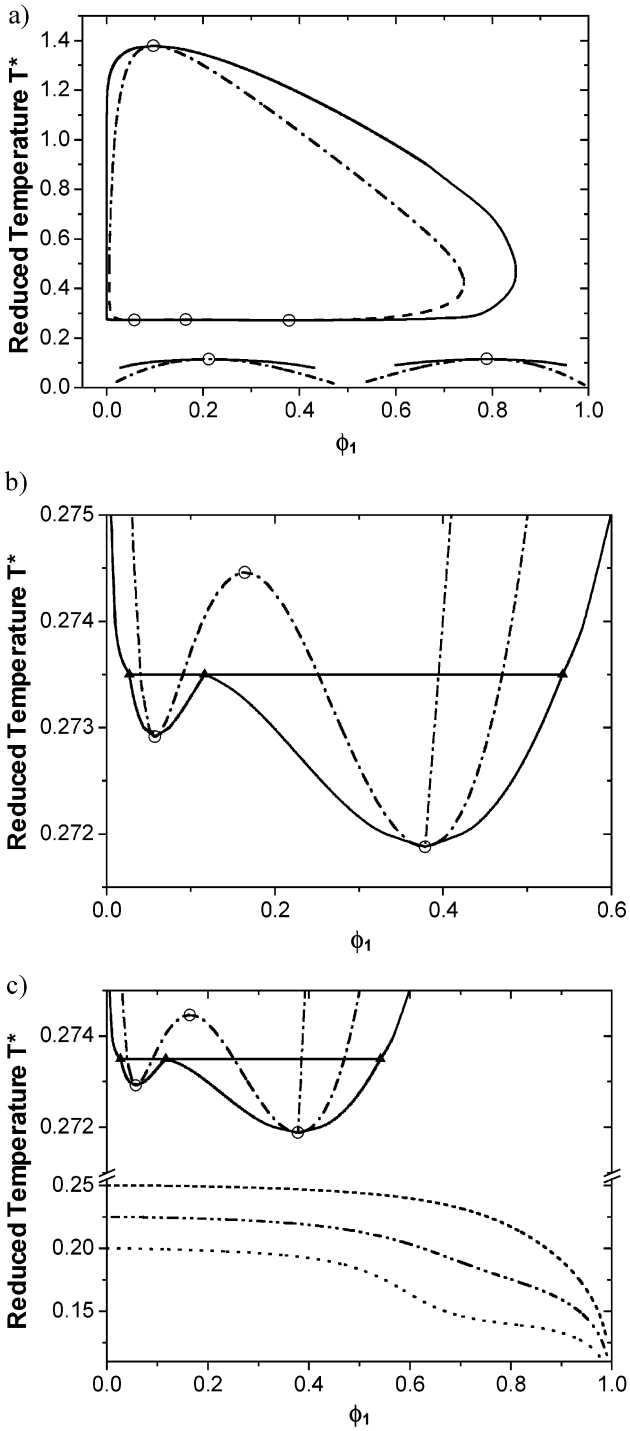

Figure 1. Theoretical reduced temperature−composition (T^*−ϕ_1) phase diagram of the model polymer solution. Predicted LCST spinodal (− · −), coexistence (−) curves, and critical conditions (○); predicted melting temperature $T^0_{m,0}{}^*$ of the solvent vs composition for three values of $T^0_{m,0}{}^*$:$T^0_{m,0}{}^*$ = 0.250 (- - -); $T^0_{m,0}{}^*$ = 0.225 (− · · −), and $T^0_{m,0}{}^*$ = 0.200 (···). Parameter values used are summarized in Table 1. (a) Global temperature−composition (T^*−ϕ_1) phase diagram showing closed loop and adjacent UCST miscibility gaps. (b) Details of the bimodal LCST showing the three-liquid-phases coexistence line (▲−▲−▲). (c) Details of bimodal LCST and solid−liquid melting lines. The melting lines are calculated for different values of $T^0_{m,0}{}^*$.

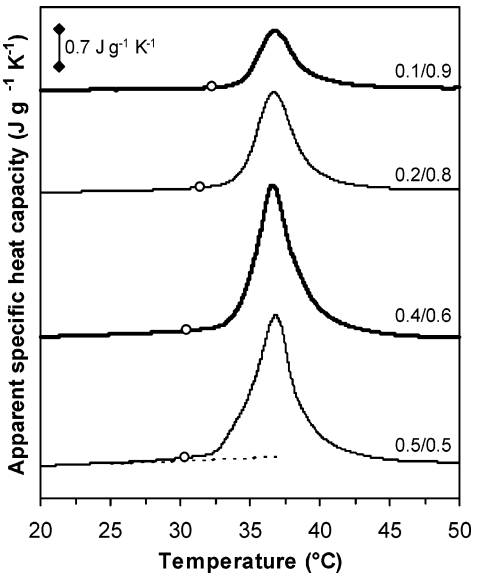

Figure 2. c_p^{app} during nonisothermal heating of different compositions PMVE/D_2O: demixing temperature (○). Extrapolated experimental c_p^{base} for 0.5/0.5 PMVE/D_2O is indicated (dashed line). Curves are shifted vertically for clarity.

of the $K_{ij}^{\alpha\beta}$ parameters, on the other hand, are not very critical for the occurrence of bimodal phase behavior. A more detailed study of the conditions leading to bimodal and other types of phase behavior (types I, II, and III)[7] will be discussed elsewhere.[25] The predicted solvent melting line is also shown in Figure 1c for different values of the equilibrium melting point of the solvent (T_m^0*), showing an unusual step with composition, which becomes more pronounced as T_m^0* is located at lower temperatures. The equilibrium melting point values of the solvent were chosen so that no interference with the LCST demixing curve took place and to demonstrate its influence on the shape of the melting line. The solvent's crystalline phase was described with standard thermodynamic correlations (eq 10).

Nonisothermal MTDSC results for PVME/D_2O. Upon heating, a PVME/D_2O mixture LCST phase separation will occur, and a considerable endothermic heat effect is observed since in the demixing process hydrogen bonds are broken and considerable compositional changes take place. Using MTDSC, the total demixing enthalpy is separated into two endothermic contributions. Usually, the largest part is found in the heat capacity signal (and as such in the reversing heat flow), whereas by construction the nonreversing heat flow contains the other part. Hence, the former signal is termed apparent (c_p^{app}) to distinguish it from the baseline specific heat capacity, c_p^{base} (see eq 11). The so-called "excess" contribution, c_p^{excess}, originates from fast reversible demixing/remixing processes at the polymer/water interphase of the coexisting phases, thoroughly elaborated in previous work:[12,16,21,38,39]

$$c_p^{app} = c_p^{base} + c_p^{excess} \tag{11}$$

Figure 2 illustrates the evolution of c_p^{app}, starting from 10 °C, for several PVME/D_2O solutions. The initial deviation of c_p^{app} regarding the extrapolated experimental baseline specific heat capacity, c_p^{base}, is considered as the start of phase separation (Figure 2, ○), as illustrated for a $w_{PVME} = 0.5$ mixture (c_p^{base} indicated by dashed line). This approach was previously discussed

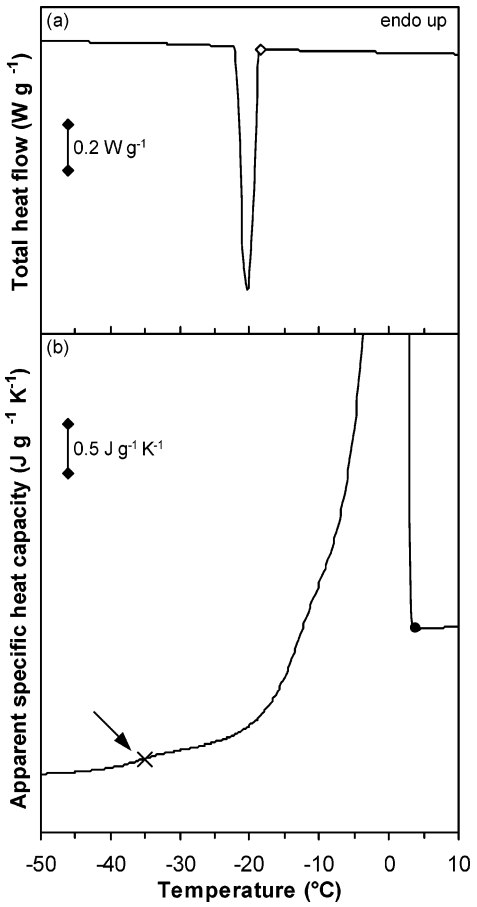

Figure 3. (a) Total heat flow during nonisothermal cooling of PMVE/D_2O 0.2/0.8: crystallization temperature (◇). (b) c_p^{app} during subsequent nonisothermal heating: T_g PVME-rich phase (×) and end set melting endotherm (●).

in more detail for the PVME/H_2O system.[16] Note that instead of using the extrapolated experimental heat capacity in order to estimate the baseline inside the phase separation region, c_p^{base} can be calculated in a more quantitative manner by considering the absolute heat capacity values of both D_2O and PVME.[40] Such detailed analysis, however, is beyond the scope of this paper.

Cooling a homogeneous PVME/D_2O solution, one expects the solvent to crystallize, as illustrated for a $w_{PVME} = 0.2$ mixture (Figure 3). Using the total heat flow signal (Figure 3a), it can be noticed that for this composition a supercooling of ca. 20 °C is needed to induce crystallization of D_2O (◇, onset crystallization exotherm), when cooling at 1 °C min^{-1}. The observed crystallization process causes phase separation, between ice crystals and a PVME-rich solution. If the crystallization would occur under isothermal conditions, it will either come to an end when the concentrated solution reaches a composition given by the solid−liquid equilibrium (at that temperature) or when the concentrated solution reaches a composition that vitrifies before the solid−liquid equilibrium composition is reached. Using nonisothermal crystallization conditions, cooling to a sufficiently low temperature, as is done in the current MTDSC experiments, will inevitably induce vitrification of the remaining concentrated polymer solution. As a result, the devitrification of that glassy PVME-rich phase is observed in the subsequent heating (Figure 3b, ×, indicated by the arrow), followed by the gradual melting of ice (Figure 3b, ●, endset melting endotherm)

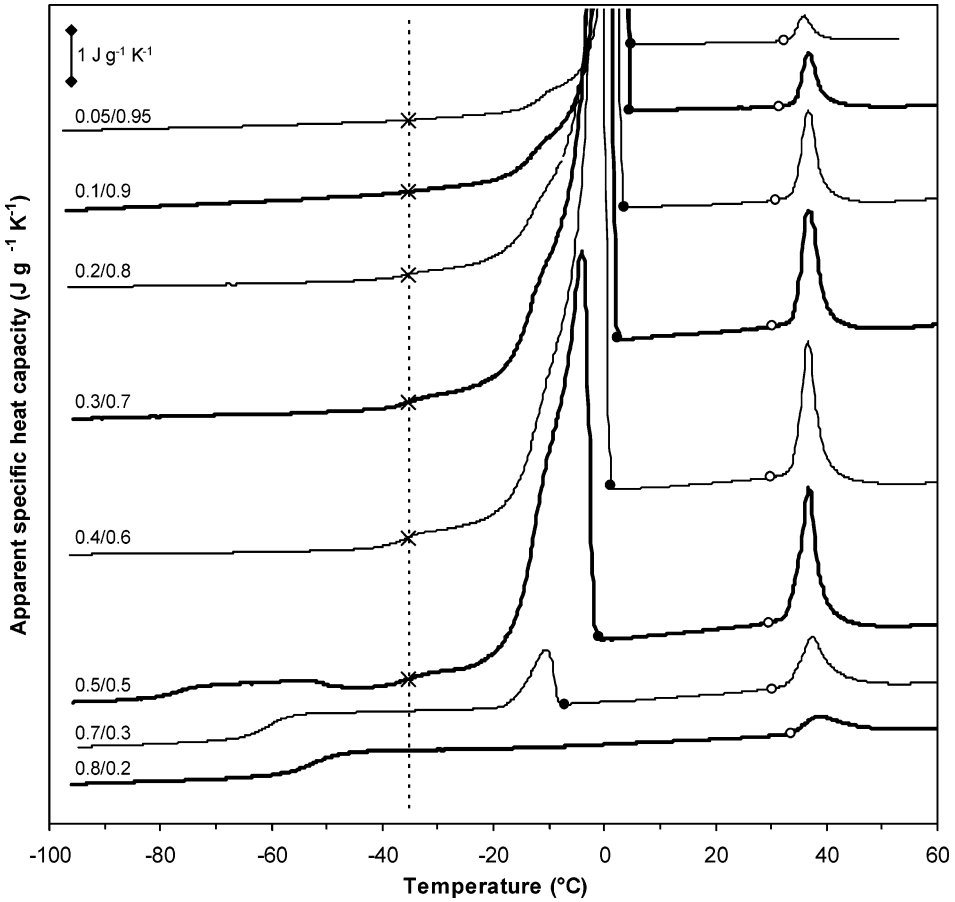

Figure 4. c_p^{app} during nonisothermal heating of different compositions PMVE/D_2O: T_g PVME-rich phase (×, vertical dashed line), end set melting endotherm (●), and demixing temperature (○). Curves are shifted vertically for clarity.

and the LCST phase separation of the remixed PVME/D_2O solution. Note that the observed glass transition temperature at ca. −35 °C corresponds to the T_g of a homogeneous solution with $w_{PVME} \approx 0.95$, which indicates that nearly all of the solvent was able to crystallize upon cooling.

Mixtures with $w_{PVME} \leq 0.6$ display crystallization upon cooling, and the melting endotherms consist of two overlapping peaks (Figures 3b and 4).[15−18] It was mentioned in the introductory part that in the case of PEO/water, for instance, such a double melting endotherm is caused by the presence of a eutectic composition.[19,20] In this case, on the other hand, such a peculiar phenomenon cannot be related to eutectic behavior as atactic PVME is unable to crystallize. The most frequently adapted interpretation of the double melting peak in PVME/water mixtures refers to the existence of bound and free water that melt at different temperatures.[17,18]

Even though crystallization upon cooling in (typical) DSC experiments solely occurs for solutions with $w_{PVME} \leq 0.6$, crystallization and melting could still be observed up to $w_{PVME} \approx 0.7$ (Figure 4), as solutions with w_{PVME} between 0.6 and 0.7 display cold crystallization upon heating. For more concentrated solutions no crystallization and thus melting could be observed (Figure 4), in agreement with literature.[15] Similar observations hold for aqueous solutions of either poly(*N*-vinylcaprolactam)[11,41] or poly(*N*-isopropylacrylamide)[10,21] in which the missing crystallization is linked to the interference of vitrification upon cooling, according to the T_g−composition curve. For that reason, the T_g of the homogeneous PVME/D_2O solutions is measured. As expected, T_g lowers with increasing D_2O content (Figure 5, indicated by the arrow), due to the plasticizing effect of D_2O on PVME. Next to the location of T_g as a function of composition (Figure 5, ■), the width of the glass transition ΔT_g is of importance as well because the possible interference of partial vitrification during crystallization depends on the upper limit of the glass

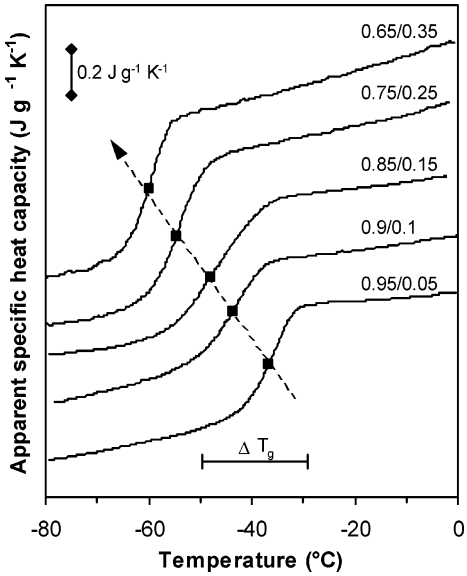

Figure 5. c_p^{app} during nonisothermal cooling of different compositions PMVE/D_2O: T_g homogeneous solution (■). Curves are shifted vertically for clarity.

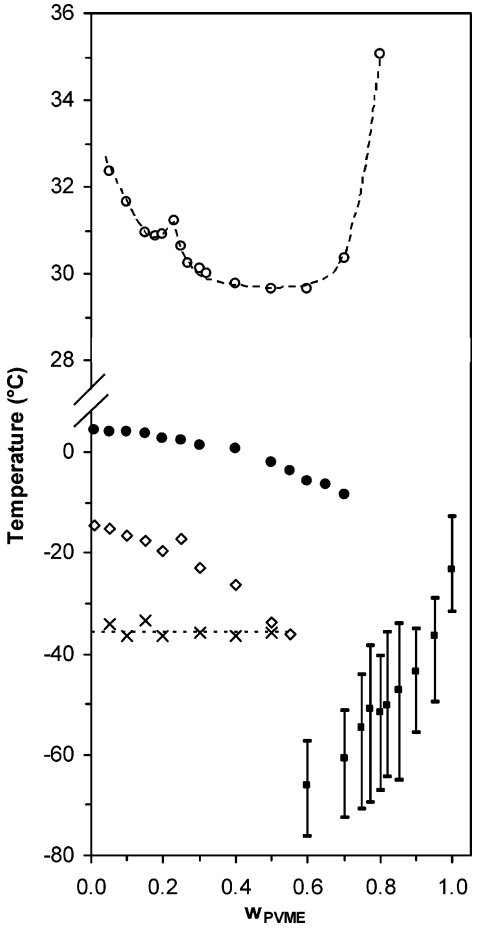

Figure 6. State diagram of PVME/D_2O determined with MTDSC: crystallization curve (◇) upon cooling; T_g PVME-rich phase (×), melting curve (●), demixing curve (○), and T_g–composition curve (■, width: I) upon heating.

transition rather than on its average value.[12,21,38] Therefore, $\Delta T_g \approx 20$ °C is indicated in Figure 5 for a mixture with $w_{PVME} = 0.95$.

State Diagram of PVME/D_2O. *Liquid–Liquid Miscibility Behavior.* The thermal transitions discussed thus far are now brought together to construct a state diagram (Figure 6), including among others the bimodal shape of the LCST demixing curve (○) together with the melting curve of ice (●) and the change of T_g with composition (■, width: I). The LCST miscibility gap in PVME/D_2O has a bimodal shape, similar to the LCST demixing curve of PVME/H_2O[15,16] and in agreement with the spinodal data from SANS.[26] As already mentioned, according to the Wertheim-LTPT, LCST bimodality is only observed when the solvent–polymer strength is (somewhat) larger than the solvent–solvent strength. It should be noted that the bimodal miscibility gap is not caused by the polymer polydispersity, as already discussed in the literature.[8,9,26] The effect of both the polymer molar mass and the associated polydispersity has been thoroughly elaborated in another paper.[39]

Furthermore, the Wertheim-LTPT also predicts the existence of two narrow, adjacent UCST's at low temperature, of which the low temperature UCST at high polymer compositions has recently been observed using SANS.[26] Unfortunately, in the MTDSC experiments presented here no heat effect associated with the UCST demixing was observed upon cooling the PVME/D_2O mixture. This is quite reasonable as the heat effects associated with variations in composition of the coexisting phases in such narrow UCST miscibility gap are expected to be much smaller compared to the heat effects observed during LCST phase separation. On the other hand, the glass transition region seems somewhat broader for compositions $0.75 \leq w_{PVME} \leq 0.90$ (Figure 6, ■, width: I), possibly indicating compositional inhomogeneities within the aqueous sample. However, the broadness of T_g is also inevitably influenced by the broad molar mass distribution of the commercially available polymer ($M_w/M_n \sim 2.5$). Therefore, to further clarify this issue, it was decided to study the phase behavior of a low molar mass PVME having a narrow polydispersity ($M_w/M_n = 1.1$).[42]

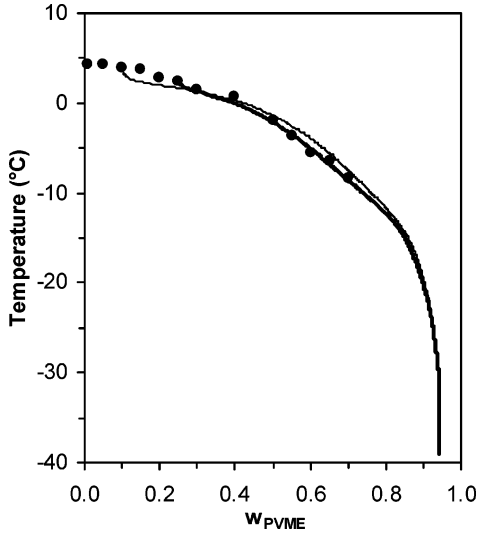

Figure 7. Change in composition with temperature for PVME/D_2O obtained by partial integration of the melting endotherm after cooling a 0.1/0.9 (thin) and 0.25/0.75 (thick) solution to −100 °C. Experimentally determined melting temperatures (●).

Solid–Liquid Behavior. The melting temperatures of D_2O determined directly by MTDSC upon heating PVME/D_2O mixtures are shown in Figures 6 and 7 (●). Apparently, they do not show a pronounced step in temperature with composition as is found in the theoretical predictions, suggesting that the melting line of D_2O resembles the predicted melting line at the highest value of T_m^0* (Figure 1). The melting of D_2O observed on heating is of course the result of the crystallization that occurred beforehand, either directly for compositions with $w_{PVME} \leq 0.6$ or via cold crystallization observed for compositions in the range $0.6 < w_{PVME} \leq 0.7$. Because of the dynamic feature of the MTDSC method, it cannot be excluded that these results do not present the real equilibrium melting line. For example, crystallization and melting of ice is not observed for concentrations larger than $w_{PVME} \approx 0.7$. This, however, does not mean that water is unable to crystallize. In fact, after the crystallization of water from the less concentrated compositions the glass transition temperature of the remaining polymer solutions is practically constant at ca. −35 °C (Figure 6, ×, horizontal dashed line) corresponding to the T_g of a homogeneous solution with $w_{PVME} \approx 0.95$. This indicates that nearly all solvent was able to crystallize upon cooling. Although the shape of the melting line determined by MTDSC does not show a pronounced step with composition, evidence for the predicted peculiar evolution of the melting line of the solvent can nevertheless be found in the (MT)DSC traces from Figure 4. The PVME/D_2O mixtures having

a composition wherein crystallization of water occurs upon cooling exhibit a melting endotherm that consists of a main peak preceded by a shoulder. The attained shape of the melting endotherm is a direct consequence of the concentration−temperature dependence of the melting of ice, being determined by the thermodynamic solid−liquid equilibrium conditions. Hence, the shape of the melting endotherm can be related, at least qualitatively, to the temperature derivative of the melting line.

Therefore, we tried to reconstruct the change in melting temperature from the shape of the observed melting peak. Indeed, assuming that the liquid D_2O formed during the melting process quickly remixes with the liquid PVME-rich phase to make the composition of the PVME/D_2O mixture in accordance with the thermodynamic solid−liquid equilibrium, the amount of heat needed up to that temperature (i.e., the partial integrated heat flow) will determine the amount of liquid D_2O formed and as such the new composition of the liquid phase in equilibrium with the remaining ice. To calculate the heat of fusion of D_2O at each temperature, accurate values of the heat capacity of deuterium oxide, in both the liquid and solid state, are needed. Since these c_p values are not as accessible as for H_2O, they were measured by adiabatic calorimetry[43] and compared to the limited number of literature data at hand.[44,45]

The resulting composition change with temperature is shown in Figure 7 for two different solutions of PVME/D_2O with $w_{PVME} = 0.1$ and 0.25, respectively. Note that the composition at low temperature starts from $w_{PVME} \approx 0.95$ because after cooling to −100 °C a vitrified mixture of such composition is formed (see Figures 4 and 6, ×). The agreement between the melting curve calculated from the shape of the melting endotherm and the melting curve determined directly from the endset temperature of the melting endotherm is reasonable but not perfect, which indicates that the assumption made about the quasi-instantaneous remixing of the freshly molten ice with the liquid PVME-rich phase only holds approximately.

Nevertheless, despite the reasonable agreement it may still be argued that the results of the dynamic MTDSC method in Figure 7 do not represent the true equilibrium melting line. Therefore, an alternative method is presented employing Fourier transform infrared spectroscopy in order to construct the equilibrium melting line spanning the entire concentration range. In this respect, we make use of the concentration dependence of the C−H symmetrical stretching absorption band of the $O-CH_3$ to directly determine the composition of the PVME/water mixture in coexistence with ice.

Equilibrium Solid−Liquid Behavior from FTIR Experiments. *The Concentration Dependence of the Position of the C−H Symmetrical Stretching Absorption Band of $O-CH_3$.* FTIR spectra were recorded in the homogeneous liquid state for samples with $0 < w_{PVME} \leq 1$, in both H_2O and D_2O. Note that the C−H symmetrical stretching absorption band displays a small dependency on temperature shifting to lower wavenumber with ca. 0.03 cm^{-1} $°C^{-1}$. To minimize the influence of this temperature dependency, the FTIR study was performed at 4 °C (0 °C) depending on the solvent used, ensuring that all mixtures were in the homogeneous liquid state. The resulting concentration dependence of the position of the C−H symmetrical stretching absorption band of $O-CH_3$ is presented in Figure 8. These results are in good agreement with earlier reported data for both PVME/H_2O and PVME/D_2O,[14] and only a small, almost negligible effect of isotopic substitution is observed (Figure 8, compare ▲ with △). The frequency of the C−H symmetrical stretching linearly shifts to lower wavenumber with increasing polymer concentration, which becomes even more pronounced at $w_{PVME} \approx 0.5$.

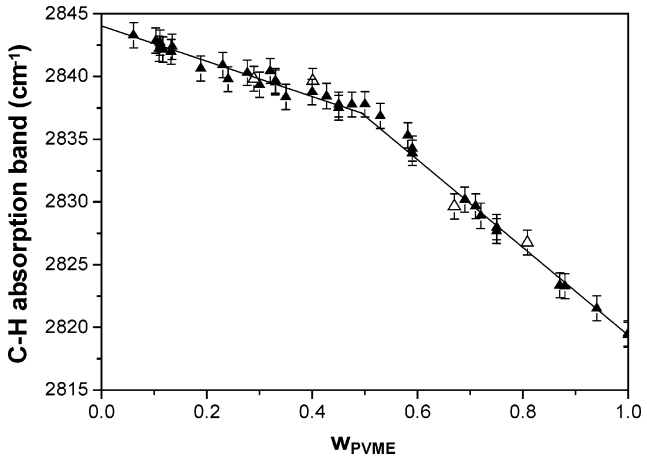

Figure 8. Concentration dependence of the position of the C−H symmetrical stretching absorption band of $O-CH_3$ in H_2O (▲) and in D_2O (△).

The Melting Line of Deuterium Oxide in PVME/D_2O. The solid−liquid behavior of D_2O was examined by following experimental procedure: a sample with, for instance, $w_{PVME} = 0.28$ for which crystallization of water readily occurs, is cooled to −40 °C at 5 °C min^{-1} and kept at that temperature to allow for maximum crystallization of D_2O, which typically is finished within 1 h. Next, the sample is stepwise heated through which at each temperature an amount of (heavy) ice melts, and the attained liquid D_2O changes the concentration of the surrounding polymer solution. This finally results in ice coexisting with a PVME/D_2O solution having a concentration according to the solid−liquid equilibrium at that temperature or the concentration of the vitrified polymer solution when vitrification occurred. After the equilibration period an FTIR spectrum is taken, and the position of the C−H symmetrical stretching absorption band of $O-CH_3$ is determined. These results are plotted vs temperature in Figure 9. Using the concentration dependence of the C−H symmetrical stretching absorption band of $O-CH_3$ (Figure 8), the wavenumber dependence in Figure 9 can be transformed in the concentration of the PVME/D_2O solution in equilibrium with ice. In this way the equilibrium solid−liquid line can be determined within the entire concentration range (Figure 10), showing a jump to lower temperatures in qualitative agreement with the predictions of the Wertheim-LTPT.

The pronounced step to ca. −10 °C near $w_{PVME} \approx 0.6$ confirms the theoretical predictions made (Figure 1) and resembles the evolution calculated from the melting endotherm (Figure 7). Note that the FTIR results most likely provide a better estimate of the true equilibrium melting line showing a well-defined step, which is essentially smeared out in the MTDSC experiment. Nonetheless, one can conclude that the double melting endotherm observed is not related to the melting at different temperatures of bound and free water as

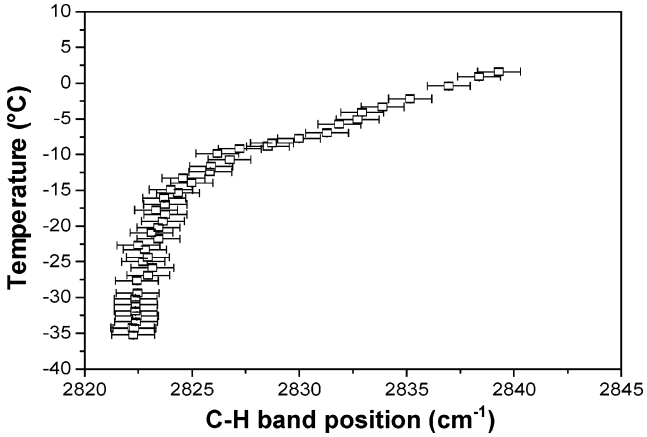

Figure 9. Position of the C−H symmetrical stretching absorption band of $O-CH_3$ against temperature (□). Details concerning the experimental procedure are given in the text.

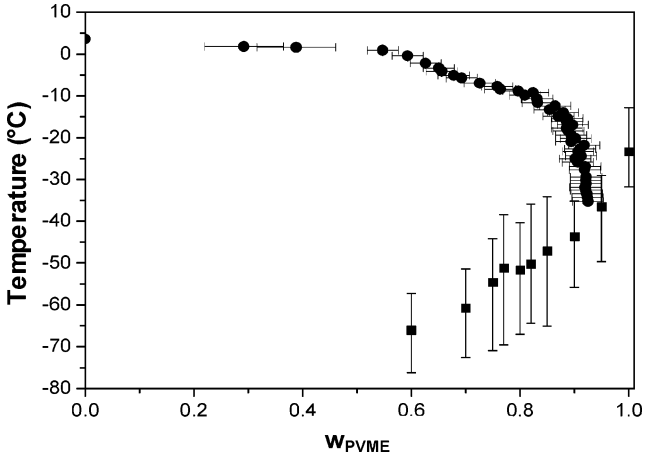

Figure 10. Melting line of D_2O in PVME/D_2O mixtures (●) from FTIR, together with the T_g−composition curve (■, width: I) from MTDSC.

suggested in the literature.[17] The experimental and predicted peculiar concentration dependence of the melting curve of ice also provides a new explanation for the inhibited crystallization at higher polymer concentrations ($w_{PVME} > 0.7$) instead of being linked to the formation of (stable) molecular complexes. That is to say, at high polymer concentration the actual supercooling becomes smaller than could be anticipated for a conventional course of the melting curve. Hence, before attaining the required supercooling the vicinity of the glass transition region dramatically slows down the nucleation rate. This observation agrees with standard polymer crystallization behavior, for which T_g largely influences the nucleation and crystallization rate.

Conclusions

The Wertheim lattice thermodynamic perturbation theory was used to predict the liquid−liquid and solid−liquid coexistence data for a model polymer solution. These theoretical predictions facilitate a far-reaching interpretation of the phase behavior of aqueous PVME solutions. The theory predicts bimodal (type III) LCST phase behavior, providing the solvent−polymer interaction strength is (somewhat) larger than the solvent−solvent strength. This bimodal LCST phase behavior was confirmed by modulated temperature DSC, using the apparent specific heat capacity signal. In addition, the solid−liquid equilibrium of the solvent was calculated, and an unusual step with composition is predicted. The composition dependence of the melting temperature of D_2O (in the presence of PVME) was either determined directly from the melting endotherm observed or calculated through partial integration, assuming immediate remixing during melting. Moreover, Fourier transform infrared spectroscopy was employed to determine the composition of the PVME/D_2O mixture coexisting with ice, using the concentration dependence of the C−H symmetrical stretching absorption band of $O-CH_3$. This FTIR method, unlike MTDSC, nearly mimics equilibrium conditions. Hence, the equilibrium melting line of D_2O was determined, corroborating its unusual step with composition.

Moreover, highly concentrated mixtures do not show crystallization and melting of D_2O, when using MTDSC. This abrupt change in crystallization and melting behavior is related to the vicinity of the glass transition temperature generating a dramatic slowing down of the nucleation rate. The peculiar concentration dependence of the melting line at high polymer concentration demonstrates that the actual supercooling becomes smaller than could be anticipated for a conventional course of the melting curve. As a result, the homogeneous solution vitrifies and nucleation of the crystalline phase does not occur. Therefore, the peculiar concentration dependence of the melting curve of ice provides a new explanation for the inhibited crystallization at high polymer concentration, which, consequently, has nothing to do with the formation of molecular complexes. Hence, the double melting endotherm observed in MTDSC is not related to the melting at different temperatures of bound and free water; it simply reflects the atypical shape of the melting line.

Finally, using the sensitivity of MTDSC in measuring glass transitions, the existence of a UCST miscibility gap at low temperature, predicted by the Wertheim-LTPT, was suggested although not confirmed yet.

Acknowledgment. Kurt Van Durme thanks the Institute for the Promotion of Innovation through Science and Technology in Flanders (IWT) for a PhD grant. Els Loozen thanks the Department of Chemistry of the Katholieke Universiteit Leuven for a PhD grant. The work was supported by the bilateral (international) scientific and technological cooperation of the Ministry of the Flemish Community and the Ministry of Science and Technology of the People Republic of China (BIL01/06). The authors thank the Fund for Scientific Research Flanders (FWO) for financial support.

References and Notes

(1) Snowden, M.; Murray, M.; Chowdry, B. Z. *Chem. Ind.* **1996**, *14*, 531−534.
(2) Shinohara, S.; Tajima, N.; Yanagisawa, K. *J. Intell. Mater. Syst. Struct.* **1996**, *7*, 254−259.
(3) Liu, Z.; Calvert, P. *Adv. Mater.* **2000**, *12*, 288−291.
(4) Hoffman, A. S. *Adv. Drug Delivery Rev.* **2002**, *43*, 3−12.
(5) Akashi, R.; Tsutsui, H.; Komura, R. *Adv. Mater.* **2002**, *14*, 1808−1811.
(6) Vihola, H.; Laukkanen, A.; Hirvonen, J.; Tenhu, H. *Eur. J. Pharmacol. Sci.* **2002**, *16*, 69−74.
(7) Šolc, K.; Dušek, K.; Koningsveld, R.; Berghmans, H. *Collect. Czech. Chem. Commun.* **1995**, *60*, 1661−1688.
(8) Schäfer-Soenen, H.; Moerkerke, R.; Berghmans, H.; Koningsveld, R.; Dušek, K.; Šolc, K. *Macromolecules* **1997**, *30*, 410−416.
(9) Moerkerke, R.; Meeussen, F.; Koningsveld, R.; Berghmans, H. *Macromolecules* **1998**, *31*, 2223−2229.

(10) Afroze, F.; Nies, E.; Berghmans, H. *J. Mol. Struct.* **2000**, *554*, 55−68.
(11) Meeussen, F.; Nies, E.; Verbrugghe, S.; Goethals, E.; Du Prez, F. E.; Berghmans, H. *Polymer* **2000**, *41*, 8597−8602.
(12) Van Durme, K.; Loos, W.; Du Prez, F. E.; Van Mele, B. *Polymer* **2005**, *46*, 9851−9862.
(13) This description assumes the polymer to be monodispers so that the polymer solution can be treated as a strictly binary system. Synthetic polymers are always polydispers and should therefore be treated as quasi-binary systems. In the quasi-binary treatment coexistence curves become cloud point curves; the three-phase line becomes a three-phase region, etc. More details on quasi- and strictly binary systems can be found elsewhere: Koningsveld, R.; Stockmayer, W. H.; Nies, E. *Polymer Phase Diagrams*; Oxford University Press: Oxford, UK, 2001.
(14) Maeda, H. *J. Polym. Sci., Part B: Polym. Phys.* **1994**, *32*, 91−97.
(15) Meeussen, F.; Bauwen, Y.; Moerkerke, R.; Nies, E.; Berghmans, H. *Polymer* **2000**, *41*, 3737−3743.
(16) Swier, S.; Van Durme, K.; Van Mele, B. *J. Polym. Sci., Part B: Polym. Phys.* **2003**, *41*, 1824−1836.
(17) Zhang, J.; Teng, H.; Zhou, X.; Shen, D. *Polym. Bull.* **2002**, *48*, 277−282.
(18) Zhang, J.; Bergé, B.; Meeussen, F.; Nies, E.; Berghmans, H.; Shen, D. *Macromolecules* **2003**, *36*, 9145−9153.
(19) Hey, M. J.; Ilett, S. M. *J. Chem. Soc., Faraday Trans.* **1991**, *87*, 3671−3675.
(20) Graham, N. B.; Zulfiqar, M.; Nwachuku, N. E.; Rashid, A. *Polymer* **1989**, *30*, 528−533.
(21) Van Durme, K.; Van Assche, G.; Van Mele, B. *Macromolecules* **2004**, *37*, 9596−9605.
(22) Wertheim, M. S. *J. Stat. Phys.* **1984**, *35*, 19−34.
(23) Wertheim, M. S. *J. Stat. Phys.* **1984**, *35,* 35−47.
(24) Chapman, W. G.; Jackson, G.; Gubbins, K. E. *Mol. Phys.* **1988**, *65*, 1057−1079.
(25) Nies, E., manuscript in preparation.
(26) Nies, E.; Ramzi, A.; Berghmans, H.; Li, T.; Heenan, R. K.; King, S. M. *Macromolecules* **2005**, *38*, 915−924.
(27) Loozen, E.; Van Durme, K.; Van Mele, B.; Berghmans, H.; Nies, E. *Polymer*, submitted for publication.
(28) Spěváček, J.; Hanyková, L.; Ilavskỳ, M. *Macromol. Symp.* **2001**, *166*, 231−236.
(29) Takada, M.; Okana, K.; Kurita, K.; Furusaka, M. *Kobunshi Robunshu* **1994**, *51*, 689−693.
(30) Okano, K.; Takada, M.; Kurita, K.; Furusaka, M. *Polymer* **1994**, *35*, 2284−2289.
(31) An, S. W.; Thomas, R. K.; Forder, C.; Billingham, N. C.; Armes, S. P.; Penfold, J. *Langmuir* **2002**, *18*, 5064−5073.
(32) Jinnai, H.; Smalley, M. V.; Hashimoto, T.; Koizumi, S. *Langmuir* **1996**, *12*, 1199−1203.
(33) Karlström, G. *J. Phys. Chem.* **1984**, *89*, 4962−4964.
(34) Qian, C.; Mumby, S. J.; Eichinger, B. E. *J. Polym. Sci., Part B: Polym. Phys.* **1991**, *29*, 635−637.
(35) Qian, C.; Mumby, S. J.; Eichinger, B. E. *Macromolecules* **1991**, *24*, 1655−1661.
(36) Horst, R. *J. Phys. Chem. B* **1998**, *102*, 3243−3248.
(37) Wolf, B. A. *Macromolecules* **2005**, *38*, 1378−1384.
(38) Van Durme, K.; Verbrugghe, S.; Du Prez, F. E.; Van Mele, B. *Macromolecules* **2004**, *37*, 1054−1061.
(39) Van Durme, K.; Bernaerts, K. V.; Verdonck, B.; Du Prez, F. E.; Van Mele, B. *J. Polym. Sci., Part B: Polym. Phys.*, submitted for publication.
(40) Pyda, M.; Van Durme, K.; Wunderlich, B.; Van Mele, B. *J. Polym. Sci.*, Part B: Polym. Phys. **2005**, *43*, 2141−2153.
(41) Kirsh, Y. E.; Yanul, N. A.; Kalninsh, K. K. *Eur. Polym. J.* **1999**, *35*, 305−316.
(42) Van Durme, K.; Van Assche, G.; Nies, E.; Van Mele, B. *Macromolecules*, submitted for publication.
(43) Smirnova, N. N.; Bykova, T. A.; Van Durme, K.; Van Mele, B. *J. Chem. Thermodyn.*, in press.
(44) Long, E. A.; Kemp, J. D. *J. Am. Soc.* **1936**, *58*, 1829−1834.
(45) Haida, O.; Suga, H.; Seki, S. *J. Glaciol.* **1979**, *22*, 155−164.

MA051745Y